O. Leav, B. Cazzolato, and C. Howard
Sound propagation through elevated, heated jets in cooler cross-flow: An experimental study
Journal of the Acoustical Society of America, 2021; 150(1):82-93

JASA ARTICLE

Sound propagation through elevated, heated jets in cooler cross-flow: An experimental study

O. Leav,[a] B. Cazzolato,[b] and C. Howard[c]
School of Mechanical Engineering, University of Adelaide, Adelaide, Australia

ABSTRACT:
Sound propagation through hot exhaust plumes with cooler cross-winds is present in many real world systems. One particular example is the sound propagation from exhaust stacks attached to open cycle gas turbine power stations. The research presented in this paper investigates the sound propagation from a reduced-scale exhaust stack, with a cross-flow from experiments conducted in a wind tunnel. Experimental measurements of the flow and temperature fields provide insight into the complex sound radiation characteristics. Results from the acoustic measurements show the change in the sound directivity arising from the inclusion of the hot exhaust plume, leading to non-axisymmetric sound directivity and a concentration of sound downwind of the exhaust stack outlet. In certain cross-flow conditions, the hot exhaust plume can increase the sound observed downwind by up to 11 dB when compared to the scenario of sound propagation from an exhaust stack in the absence of a heated jet or cross-flow. This paper describes the acoustic directivity at various radial distances from the exhaust stack, acoustic frequencies, jet temperatures, and cross-flow free-stream velocity. The results from this paper emphasise the importance of taking into consideration the hot exhaust plume with cooler cross-flow when estimating sound levels downwind of the stack.
 https://doi.org/10.1121/10.0005489

(Received 19 September 2020; revised 1 June 2021; accepted 9 June 2021; published online 7 July 2021)

[Editor: James F. Lynch] Pages: 82–93

I. BACKGROUND

Outdoor sound propagation models commonly use monopole radiators, and predicted sound levels at a receiver depend on a number of factors including the atmospheric conditions, the acoustic properties of the ground, the terrain, and geometry between source and receiver. Many models fail to capture near-field aero-acoustic phenomena, which can be an issue in high thermal or velocity gradients. An example of such a case is sound radiation from open-cycle gas turbines (OCGT), which has been shown in the literature to produce higher than expected low frequency noise levels in communities,[1–10] especially within the range from 16 to 63 Hz. It has been reported that the low frequency noise levels from OCGT have caused the following impact on communities: perceived "annoyance" or throbbing,[4] "beating" sensation in the chest,[5,6,10] nausea,[4] and acoustic excitation in structures with low resonance frequencies.[4,10] These high community noise levels observed from OCGT are not typically seen in combined cycle gas turbines, which use both Brayton and Rankin cycles and thus the exhaust is at lower temperatures, which improves the effectiveness of absorptive silencers.[1,7]

Sound levels in neighbourhoods near exhaust stacks are commonly predicted using multiple ISO standards.[11–13] ISO 10494:2018[13] is used to estimate the sound power and sound pressure levels (SPLs) from exhaust stacks. The sound propagation is modelled using ISO 9613-1:1993[11] and ISO 9613-2:1996.[12] For simple sound predictions, ISO 9613-2:1996[12] states that a simple monopole source can be used, but for more complex sound sources, a directivity correction factor can be applied. If a single monopole source cannot be used, then multiple monopole sources can be used to represent a discretised line source or discretised area source. A single value correction factor based on the meteorological conditions obtained from the "local authorities" can be applied to the sound propagation model. These sound prediction models can also be extended using numerical software to include the atmospheric boundary layer (thermal and velocity gradients) and complex terrains. There are also several literature reviews[14–19] on the topic of quantifying atmospheric sound propagation, which involves more sophisticated numerical modelling techniques for predicting sound in the far-field. However, these atmospheric sound propagation models do not take into consideration the complex sound field from the exhaust stack and the acoustic interaction with the exhaust plume.

Hot stacks may be classified as an elevated jet in cross-flow (JICF), which is shown schematically in Fig. 1. The elevated JICF is a cylindrical duct protruding from a ground-plane, with a jet flow exiting the duct. The flow structures associated with isothermal elevated JICF have been studied experimentally by various researchers,[20–26] and to a lesser extent, non-isothermal elevated JICF have also been investigated.[27–29] The fluid structures are governed by the JICF momentum flux ratio, defined as

[a]Electronic mail: orddom.leav@adelaide.edu.au, ORCID: 0000-0003-0903-9553.
[b]ORCID: 0000-0003-2308-799X.
[c]ORCID: 0000-0002-7677-5318.

 0001-4966/2021/150(1)/82/12/$30.00

https://doi.org/10.1121/10.0005489

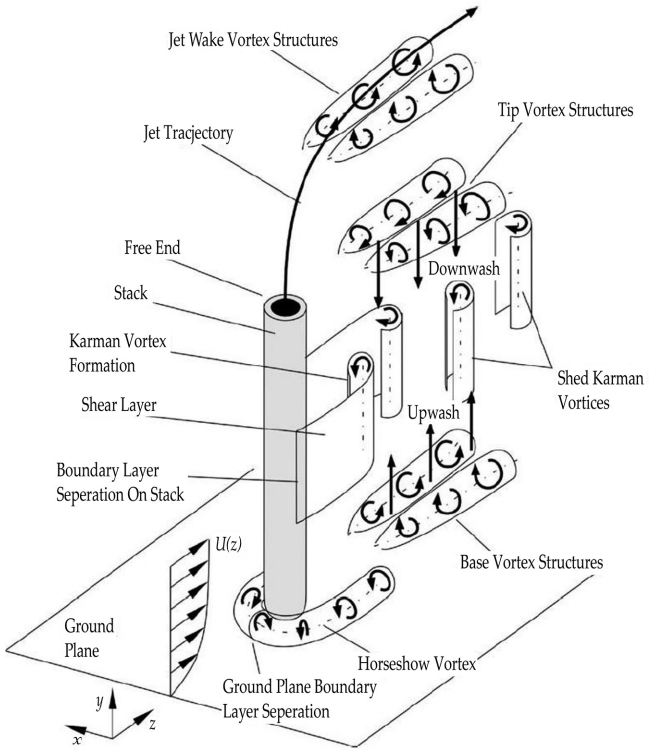

FIG. 1. Schematic of the dominant fluid dynamic structures associated with an elevated JICF for a value of R that is in the jet dominated regime (Ref. 20).

$$R = \sqrt{\frac{\rho_j u_j^2}{\rho_{cf} u_{cf}^2}}, \tag{1}$$

where ρ_j is the jet air density, ρ_{cf} is the cross-flow free stream air density, u_j is the average jet exit velocity, and u_{cf} is the cross-flow free stream velocity. The values for R in OCGTs are typically in a "jet-dominated" regime.[20,24,25,29] The unique flow structures that form in this regime are the following: deflected jet, jet shear layer, counter rotating vortex pairs, and stack shear layer.[20]

Research has shown that the sound radiation from exhaust ducts is often quite complex. One of the earliest studies for sound radiation from gas turbine exhaust stacks was conducted by Wells and Crocker,[30] where they investigated the sound radiation from an exhaust duct in the absence of flow and temperature. This was an analytical and experimental study that presented directivity results of an axisymmetric sound radiation with an acoustic lobe forming on-axis at 0°. Similar experimental studies have been conducted,[31–33] with sound radiation from exhaust ducts in the absence of flow in an anechoic environment that showed a similar outcome with a lobe forming on-axis as the acoustic frequency increased.

When the exhaust from a stack enters the atmosphere, a jet shear layer forms, and it is known that this causes sound refraction to occur.[34,35] The sound refraction due to the shear layer can be extended to non-isothermal jet shear layers, showing significant sound refraction.[36–38] The change in sound directivity from sound refraction becomes more pronounced with an increase in jet Mach number M_j, jet temperature T_j, and acoustic frequency. Mungur *et al.*[39] showed that for isothermal jets, the location at which the sound directivity measurements are taken is important, with the developing jet shear layer downstream causing continual refraction at increasing duct diameters ($2D - 40D$, where D is the duct diameter) from the exhaust outlet. Cummings[40] conducted an experimental study of a reduced-scale boiler flue-gas stack, where he investigated the radiation impedance and transmission loss for an unflanged exhaust duct with a heated exhaust jet ($T_j = 300\,°\text{C}$). Further numerical work was undertaken by Astley and Eversman,[41] using similar test parameters as Cummings,[40] and used the transmission loss at the duct opening as validation. Using an acoustic finite element (FE) solver and the Helmholtz equation, Astley and Eversman[41] showed with sound directivity results that refraction of sound occurs from a heated jet at varying directivity radii ($1D < r < 40D$) and a Helmholtz number, ($ka = 2.0$, where k is the wavenumber and a is the duct radius). Such work on jet shear layer refraction was also extended to OCGT exhaust flow with near-field ($r < 3D$, where r is the directivity radius and D in the internal diameter) measurements by Björk,[1] which showed that sound is refracted by the jet shear layer and this was measured in both a real OCGT exhaust stack and in a scaled model.

Björk[1] proposed that sound radiating from OCGT exhaust stacks form strong lobes, and that under certain meteorological conditions, leads to the amplification of sound downstream as it interacts with the bent-over hot exhaust plume. Earlier work by Björk,[1] stated that a bent-over hot exhaust plume with the thermal gradients and varying wind conditions would cause variations in sound levels downstream of up to ±5 dB in the neighbourhood. However, Björk[1] only measured the sound in the near field; from the real exhaust stack at approximately $1.5D$ and approximately $3D$. In the near-field, the onset of refraction begins and cross-flow effects are yet to occur. Previous numerical studies by Leav *et al.*[42,43] showed that the propagation path of sound is affected by the temperature of the plume for both a two-dimensional (2-D) non-isothermal ground-level JICF, and for a three-dimensional (3-D) elevated JICF. They have also shown that the propagation path of sound is dependent on the acoustic frequency and the distance from the exhaust outlet. Upstream of the exhaust stack, the sound remains relatively unaffected by the cross-wind, with elliptical acoustic spreading observed.[43] However, downstream of the exhaust stack, the sound field forms a highly directed lobe of sound.

This paper contains results from experimental investigation of the sound directivity of an elevated hot exhaust jet in cooler cross-flow. A reduced scale (1:125) experimental rig is used to emulate the flow and acoustic conditions of a 190 MW OCGT. This was tested at the University of Adelaide's Wind Tunnel under three different flow conditions described in Fig. 2. The experimental findings from the reduced scale experiments are used to analyse the effects

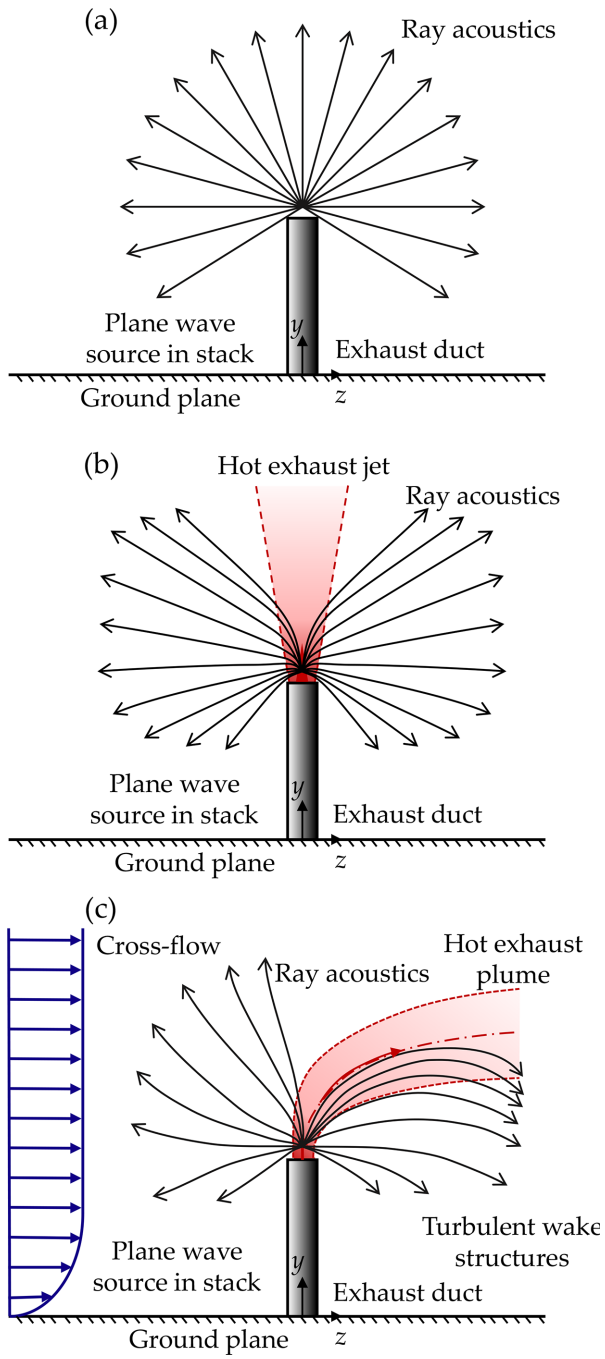

FIG. 2. (Color online) Schematics of the three experimental testing regimes in the Adelaide Wind Tunnel; (a) sound propagation through the exhaust stack in a stagnant flow, (b) sound propagation through a heated jet with no cross-flow, and (c) sound propagation through a non-isothermal heated JICF.

of the plume on the propagation of sound. The layout of the paper is as follows. A description of the experimental setup and the signal processing techniques used for the acoustic and flow measurements are discussed in Sec. II. The flow and temperature measurements are presented and discussed in Sec. III. In Sec. IV, the acoustic directivity measurements are detailed. The main conclusions of the paper are summarised in Sec. V.

II. EXPERIMENTAL APPARATUS AND METHODOLOGY

Experiments on real OCGT are difficult due to the practicality of controlling flow and speed, as well as taking measurements to characterise flow temperature, flow speed, and sound pressure. The aim of this research is to simulate the flow, temperature, and acoustic parameters of a full-scale 190 MW OCGT (SGT5-2000E from Siemens[44]) with a small-scale rig of an exhaust stack where the relevant parameters can be controlled. This section will discuss the experimental apparatus representing the OCGT, the commissioning of the experimental apparatus at the University of Adelaide Wind Tunnel, shown in Fig. 3(a), instrumentation, and the signal processing techniques used to process the acoustic data.

The experimental apparatus for simulating the exhaust flow and sound is shown in Fig. 3(b). Table I shows the non-dimensional parameters relevant to full-scale OCGTs used for the exhaust rig. The values used in Table I are based on a 190 MW OCGT from Siemens (SGT5–2000E),[44] and the experimental setup is approximately 1 : 125 scale. An important note is that, ka, the Helmholtz number is dependent on, c_j, the speed of sound of the jet with different jet temperature. A centrifugal blower (Leister Airpack) was used to generate the flow in the duct network. The inlet and outlet of the blower were connected to acoustic silencers to minimise the sound from the blower affecting acoustic measurements. The flow travelled through a constant thickness stainless-steel duct network with an outer diameter of 50.8 mm and an inner diameter of $D = 47.6$ mm ($D = 2a$). This leads to the exhaust duct wall contributing to 6.3% of the overall cross-sectional area and due to the relatively thin duct walls, the impact of edge diffraction and contribution to the instability of the vortex sheet of the jet would present minimal impact on the results. The flow from the outlet silencer to the Airpack blower was split into a Y-junction and was passed through two 16 kW Leister 61 L System Air Heaters capable of variable temperature control, and then joined again with a 45° Y-junction into a single flow. Two heaters were used in lieu of a single unit due to the lower cost and practicality of delivering two lower amperage three-phase power, rather than a single high amperage three-phase power which was unaffordable and unavailable. The flow in the duct network was measured with a pitot tube coupled to a differential pressure transducer (ManyYear Technology MPT-721). The temperature in the duct network was measured using k-type thermocouples. The flow then passed through a 90° bend to change the direction of flow to vertical before entering an automotive catalytic converter, which is comprised of Corning Celcor with square pores, that acted to straighten the flow. The flow beyond the catalytic converter passed through a straight vertical section of pipe before exiting as a jet. The exhaust network was clad with Rockwool sectional pipe insulation to reduce the heat loss in the pipe network and attenuate structural acoustic radiation.

Figure 3(c) shows a photograph of the experimental setup in the University of Adelaide's Wind Tunnel. A

https://doi.org/10.1121/10.0005489

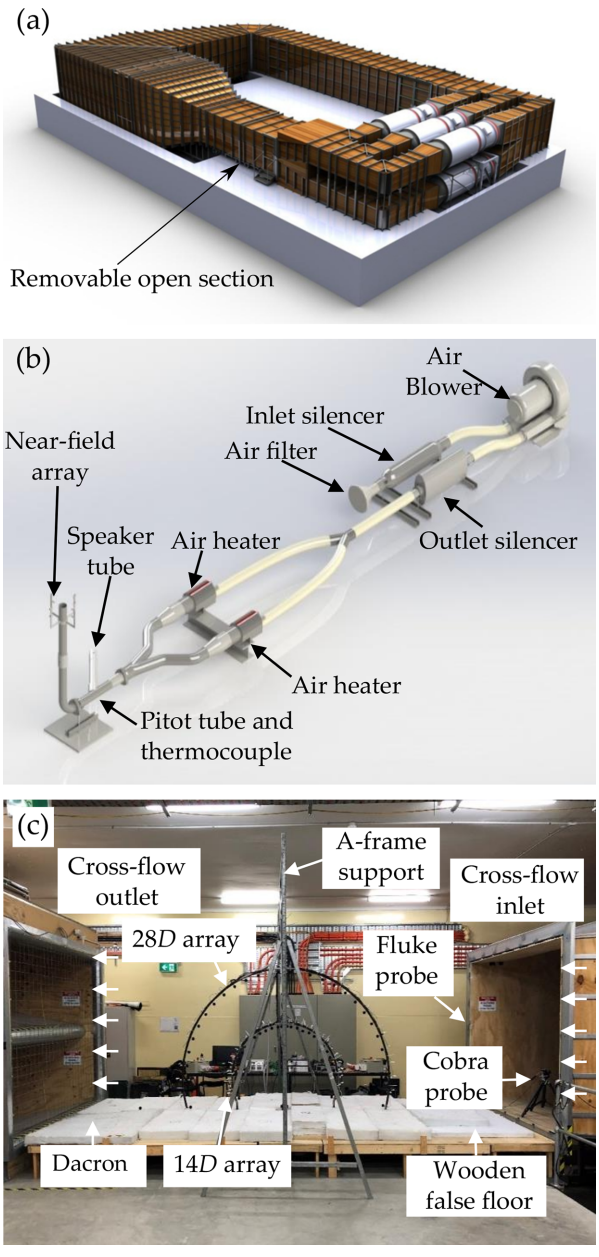

FIG. 3. (Color online) Images showing (a) the closed-loop four-sided University of Adelaide Wind and the removable test section, (b) an illustration of the reduced-scale exhaust network experimental setup, and (c) a photo of the experimental set up at the University of Adelaide's Wind Tunnel showing the full span of the commissioned test set up.

wooden decking acting as a ground-plane was placed over the exhaust rig. Acoustic foam (50 mm thick Dacron) was placed on the wooden decking to reduce acoustic reflections from the ground plane and to provide an anechoic surface above 500 Hz, thereby reducing the complexity of the sound field so that the effect of the plume, cross-flow, and sound interaction could be examined. The wooden decking is used so that only the exhaust stack interacts with the flow, with the rest of the apparatus shielded from the flow. The cross-sectional area of the wind tunnel cross-flow is 2.75 m × 2 m and the available test section ground area covers a span of 3.5 m × 5.5 m. The cross-flow wind velocity was measured

TABLE I. Physical parameters for the experimental tests, where parameters with the subscript $_j$ corresponding to the jet and subscript $_{cf}$ corresponding to the cross-flow.

Parameters	Equation/expression	Value	Units
Duct diameter	D	47.6	mm
Duct length	$L = 10D$	476	mm
Jet temperature	T_j	300-773	K
Momentum flux ratio	$R = \sqrt{\frac{\rho_j u_j^2}{\rho_{cf} u_{cf}^2}}$	5–12.5	
Cross-flow wind speed	u_{cf}	0–7	Ms^{-1}
Helmholtz number	$ka = \frac{\pi f D}{c_j}$	0.85–1.70	—
Mach number	$M = \frac{u_j}{c_j}$	0.1	—

with a Cobra Probe 209 and a Fluke 922 airflow meter at discrete points in the cross-flow free-stream velocity.

The sound pressure was measured with 62 1/4 in. G.R.A.S. 40PH Free-Field Microphones along two circular arrays with radii 14D and 28D from the exhaust stack outlet. The microphones, according to the manufacturer, have a flat frequency response (±1 dB) within a frequency range of 20 Hz to 10 kHz. Microphone wind screens (G.R.A.S. AM0071 Windscreen) designed for the 1/4 in. G.R.A.S. 40PH Free-Field Microphones were used to minimise the flow induced noise. It should also be noted that further signal processing of the acoustic measurements was undertaken to minimise the effects of flow induced noise from measuring the acoustic pressure in the wind tunnel with the jet flow and cross-flow present, which are detailed later in the paper. The microphones in Fig. 3(c) were placed along a circular arc spanning ±210°, with each microphone spaced at 7.5° increments, except for the centre microphone at 0° being replaced by two microphones at ±2.5° for the 14D array arc and for the 28D arc the centre microphone at 0° was removed to accommodate the vertical support. The microphone arrays were positioned parallel to the cross-flow free stream. The microphone arrays were supported by a frame, designed to have minimal flow and acoustic impact. The microphone signals were recorded by a NI (National Instruments) PXIe-4499 Sound and Vibration Module in a NI PXIe 1082 Chassis. The sound source used was uniform Gaussian white noise, generated from NI LABVIEW and the electrical signal was generated using a NI PXI-6221 Multifunction I/O Module. The sampling frequency was 25.6 kHz. The uniform white noise was passed through a dual channel analogue 4-pole Butterworth filter (Krohn-Hite model 3362 Dual Channel Filter) designed with low-pass and high-pass filter to generate one-third octave bands over several frequencies (f = [3150, 4000, 5000, 6300 Hz] or $ka = [0.85, 1.08, 1.35, 1.70]$). The sound was generated using two compression drivers, a 50.8 mm (2 in.) DS18 PRO-DKH1 1000 W compression driver and the 50.8 mm (2 in.) TIMPANO TPT-DH2000 400 W compression driver to deliver relatively uniform sound power over the desired bandwidth.

The acoustic data were post-processed in the frequency domain using MATLAB. The spectral analysis used a Hanning window with an fast Fourier transform length of 4096 and 1500 averages. Post-processing of the measurement data using Coherent Output Power (COP), described by Bendat and Piersol,[45] improves the signal-to-noise ratio of the experimental measurements and can reveal important acoustic features of the system under investigation. The degree of linearity between the acoustic-electrical signal generated by the data acquisition system (x) and the acoustic pressures measured at the microphones (y) may be quantified using the coherence function,

$$\gamma_{xy}{}^2(f) = \frac{|G_{xy}(f)|^2}{G_{xx}(f)G_{yy}(f)}, \tag{2}$$

where f is the frequency of interest, G_{xy} is the cross-power spectra of the acoustic-electrical signal into the speaker and the microphone acoustic pressures, G_{xx} is the power spectra of the acoustic-electrical signal into speaker, and G_{yy} are the power spectra of the microphone acoustic pressures.[45] The results in this paper are presented as the COP at each microphone given by

$$\mathrm{COP}(f) = G_{yy} \times \gamma_{xy}{}^2. \tag{3}$$

The acoustic COP was used, rather than the raw SPLs, so that only sound correlated with the loudspeaker is analysed, and thus noise from the blowers, wind tunnel fan, and flow induced noise is removed. Moreover, comparisons were made with the compression drivers on and off (background), which demonstrates that the noise from the compression drivers were from 20 to 40 dB higher than the background. Investigating γ_{xy}^2 has shown that the coherence exceeded 95% in all the cases presented in this study and the noise from other sources contributed to less than 5% of overall acoustic energy at the microphone locations. The acoustic results for directivity presented in Sec. IV are calculated as

$$\mathrm{DI}(f,\theta) = \frac{\mathrm{COP}(f,\theta)}{\mathrm{COP_{av}}}, \tag{4}$$

where DI is the directivity index based on the acoustic COP and not the standard formulation involving sound intensity,[31] θ is the angular position from the centreline of the duct, and $\mathrm{COP_{av}}$ is the average acoustic COP along the directivity arc. This method of presenting the coherent results was chosen to ensure that the sound field presented was coherent with the loudspeaker only, and the incoherent sound from external sources was "screened out" and not considered.

An important note is that experiments were also conducted with only half of the downwind microphone array (105°). When compared to the full array, upwind and downwind of the exhaust stack, the inclusion of the microphone array upwind of the exhaust stack presents no discernible effect on the results. Additionally, the maximum cross-flow speeds was $7\,\mathrm{ms}^{-1}$, which leads to a Mach number of approximately 0.02 and since dipole noise has an SPL that is typically associated with U^6, the low cross-flow speeds suggest that the flow generated noise is insignificant.

The flow and temperature measurements were conducted for the reduced-scale exhaust rig in the Adelaide Wind Tunnel. Figure 4 shows the experimental setup for measuring flow and temperature. A Dantec three-axis traverse was used to accurately position the flow and temperature instrumentation. The flow velocity was measured with a Cobra Probe 209 at various positions in the flow and a Fluke 922 airflow meter was placed at a fixed position upwind of the exhaust stack as a reference velocity for the cross-flow. The Cobra Probe 209 is a dynamic multi-hole pressure probe that can measure all three Cartesian velocity components, and the corresponding pressures. The air velocity measurements from the Cobra Probe 209 were used to calculate the cross-flow free-stream velocity (w) and the turbulence intensities (TI) using

$$I_{ww} = \frac{\sqrt{\overline{w'^2}}}{\bar{V}} = \frac{\sigma_w}{\bar{V}}, \tag{5}$$

where w' is the fluctuating cross-flow free-stream velocity, and σ_w is the standard deviation of the cross-flow free-stream velocity.

It should be noted that there are limitations in measuring the velocities using a Cobra Probe 209. Due to the orientation of the Cobra Probe, only positive velocities can be measured for w, the cross-flow free-stream direction. This is due to the position of the holes at the head of the Cobra Probe for pressure measurements. Therefore, reverse flow measured for w saturates the signal and returns $0\,\mathrm{ms}^{-1}$ for those measurements. Note that the traverse arm is situated behind the Cobra Probe, and any reverse flow measurement would be compromised by the traverse. Additionally, the velocity limit of the sensor was $35\,\mathrm{ms}^{-1}$, and this velocity

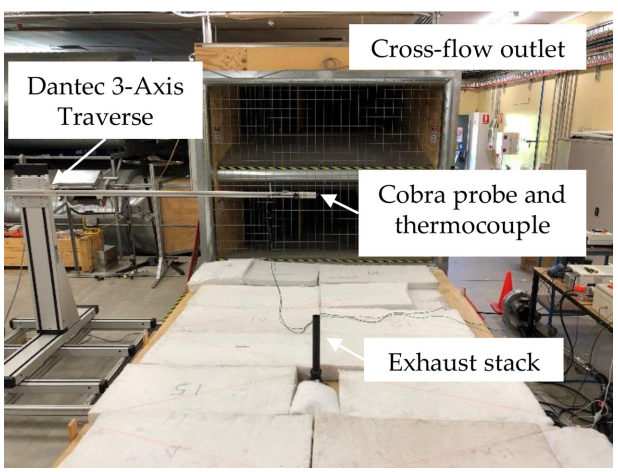

FIG. 4. (Color online) Photo of the exhaust rig, the Dantec 3-Axis traverse for flow and temperature measurements at the University of Adelaide Wind Tunnel.

https://doi.org/10.1121/10.0005489

limit is near the maximum velocity of the isothermal jet, with Mach number 0.1. It should be noted that velocity measurements near the duct outlet may exceed the velocity limits.

Temperatures outside the duct and in the domain were measured using three k-type thermocouples. The three unique positions of the thermocouples are upwind of the exhaust stack at the Fluke 922 airflow meter, at the end of the Dantec three-axis traverse with the Cobra Probe 209, and downwind of the exhaust stack at the cross-flow outlet of the Adelaide Wind Tunnel. Due to the limitations of the wind tunnel, the ambient cross-flow temperature could not be held constant throughout the testing campaign. Testing was conducted on days with large temperature variations, with cross-flow temperatures varying from 26 to 36 °C. The large changes in temperature were not evident for small durations of measurements but were evident over multiple hours. Hence, to account for changes in the ambient temperature, a dimensionless temperature parameter, based on an equation from Kamotani and Greber[46] was used, and defined as

$$\Theta = \frac{T - T_{cf}}{T_j - T_{cf}}, \tag{6}$$

where T is the measured temperature from the thermocouple at a point, T_j is the jet temperature from a thermocouple in the duct, and T_{cf} is the measured cross-flow temperature. The main difference in Eq. (6) and the equation in Kamotani and Greber[46] is that T_j is replaced with T_{max}, which is the maximum temperature measured in that particular temperature profile or temperature contour plane.

III. FLOW AND TEMPERATURE RESULTS

The experimental flow and temperature measurements for the reduced-scale elevated exhaust JICF are presented in this section for two different cases: isothermal (jet and cross-flow at identical ambient temperatures) and non-isothermal (heated jet in cooler cross-flow) JICF. The first set of results presented in this section are the flow measurements for the isothermal JICF. The second set of results discussed are the temperature measurements for the heated JICF. Flow measurements were not taken for the heated JICF to prevent the Cobra Probe 209 from being damaged by the hot plume. An important note is that the flow and temperature measurements are conducted with the microphone arrays removed.

The flow measurements are presented as vertical (varying y) profiles at various positions upwind and downwind of the exhaust stack, along the Y–Z plane intercepting the centre of the duct ($x = 0$). Additional span-wise flow measurements were undertaken with varying heights ($y/D = [17, 18, 21]$) at $z/D = 8$ downwind of the exhaust stack. The span-wise measurements were limited to only three span-wise profiles due to the limited time available for measuring the flow at the wind tunnel. The experimental flow results for this section are presented with two different flow statistics: time-averaged velocity components and turbulence intensities.

The time-averaged (Cartesian) velocity components were measured to understand the isothermal JICF bulk fluid dynamics. Figure 5(a) shows the cross-flow free-stream velocity, w, and corresponding turbulence intensities, I_{ww}, at various distances upwind and downwind of the duct outlet ($z/D = [-8, -4, 4, 8, 16]$), with the measurements along the Y–Z plane intercepting the centre of the duct ($x = 0$). For the upwind ($z/D = [-8, -4]$) velocity profiles, the velocity components are all relatively uniform, with small variations in the boundary layer. As the plume propagates downwind from the exhaust stack, from $z/D = 4$ to $z/D = 16$ the w component shows the following trends:

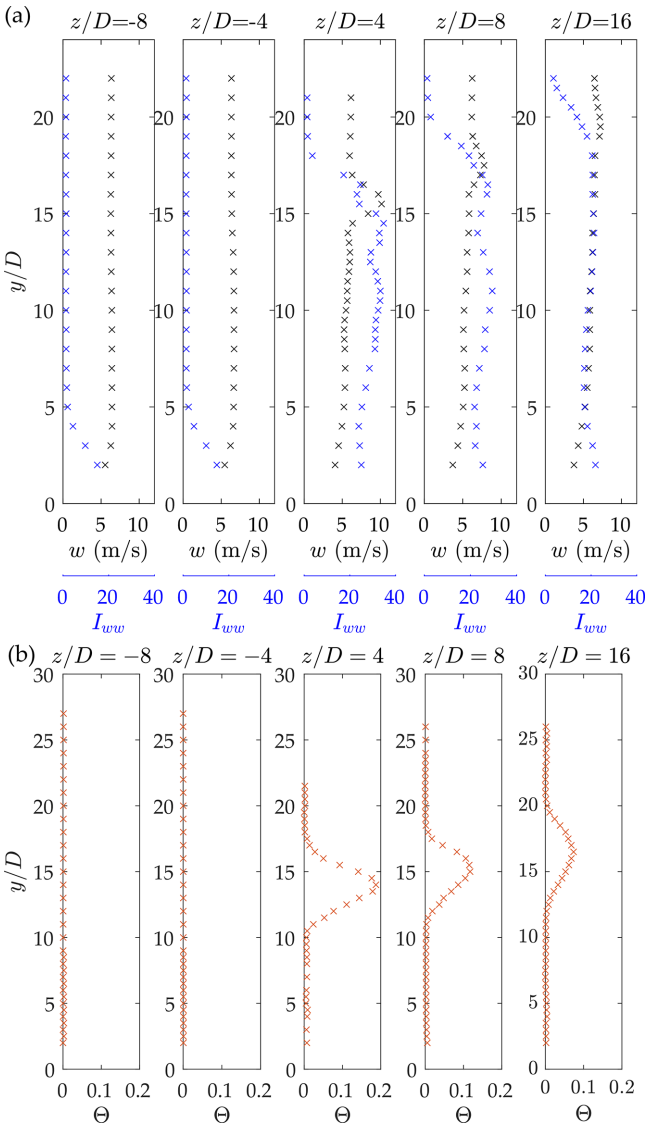

FIG. 5. (Color online) The vertical profiles for (a) w, cross-flow free-stream velocity (black crosses), and I_{ww}, turbulence intensity (blue crosses) are shown with a jet ($T_j = 27\,^{\circ}\mathrm{C}$) in cross-flow. The vertical profiles for (b) Θ, temperature (red crosses) are shown with a heated jet ($T_j = 500\,^{\circ}\mathrm{C}$) in cooler cross-flow. The vertical profiles are at varying distance downwind and upwind ($z/D = [-8, -4, 4, 8, 16]$), and measured along a plane with $x = 0$ (along the duct centreline).

- a decrease in the maximum w velocity from $w \approx 18.4\,\mathrm{ms}^{-1}$ to $w \approx 7.2\,\mathrm{ms}^{-1}$, and
- an increase in the vertical (y) size of the plume.

All trends listed are consistent with previous studies.[20,27–29] The following phenomena can explain these trends; as the plume propagates downwind, the plume spatially spreads and dissipates, with the entrainment of the cross-flow. The dissipation of the plume leads to the flow resembling the cross-flow free-stream profiles in Fig. 5(a) at $z = [-8D, -4D]$.

The incoming turbulence intensity was measured upwind of the exhaust stack to quantify the fluctuation in measured velocity. Figure 5(a) shows that upwind of the stack ($z/D = [-8, -4]$) the turbulence intensity is relatively uniform in the cross-flow free-stream and shows an increase in turbulence intensity along the boundary layer. The increase in the TI in the boundary layer is due to the vorticity present in the boundary layer. It should be noted that the cross-flow free-stream turbulence intensity upwind of the exhaust stack in the reduced-scale model is relatively low (from 0.5% to 1.5%) in comparison to the incoming turbulence intensity from atmospheric boundary layers (ABL) in nature. Hence, in real OCGTs, the diffusion of the plume is expected to be faster than the diffusion of the plume observed in this experimental study, as supported by previous studies.[27,28]

The cross-flow interacting with the elevated exhaust jet gives rise to complex features downwind of the exhaust stack due to the different flow structures that can be observed with TI measurements. Figure 5(a) shows the TI has significantly increased downwind of the duct ($z/D = [4, 8, 16]$), in comparison to upwind of the duct outlet ($z/D = [-8, -4]$). This is due to the incoming cross-flow interacting with the stack and jet to produce commonly observed fluid dynamic features, namely the plume, jet-wake, and stack-wake. There is also a distinguishing difference in TI for the plume and cross-flow free-stream, where the cross-flow free-stream TI is approximately 1%. From this, it can be ascertained that as the plume propagates the core of the plume increases in height downwind. The overall TI at $z/D = [4, 8, 16]$ reduces as the plume propagates and dissipates into the cross-flow. The TI measurements in Fig. 5(a) also show that the plume continues for the entire experimental domain and has yet to dissipate into the cross-flow. It would be ideal in the future to measure flow profiles further downwind of the exhaust stack ($z/D > 16$) to investigate distance before the plume dissipates into the cross-flow; however, this requires a larger wind tunnel, preferable anechoic.

An issue with measuring the flow in the absence of a heated jet is that the effects of buoyancy are not present. It is expected that the fluid dynamics of the plume, but in particular the position of the plume, would change slightly with the inclusion of the heated jet. However, for the purposes of this study, the flow measurements were used to show that the reduced-scale experiments reproduced salient flow features observed in the literature.[20,27,28] Moreover, the complex velocity gradients measured downwind of the exhaust stack would affect the sound radiation.

The temperature gradients downwind of the exhaust stack are complex due to the heated plume. In Fig. 5(b), the vertical (y) temperature profiles at different distances upwind and downwind of the exhaust stack are presented, with all the measurements made along the Y–Z plane that intercepts the centre of the duct ($x = 0$). A second set of temperature results are shown in Fig. 6 as contour plots along the X–Y planes at various distances downwind of the exhaust stack ($z/D = [8, 16]$).

Figure 5(b) shows that upwind of the duct outlet, the temperature is approximately uniform, with $\Theta = 0$. However, downwind of the exhaust stack, the temperature of the plume is not uniform and exhibits the following trends:

- a decrease in maximum normalised temperature from $\Theta \approx 0.19$ to $\Theta \approx 0.075$,
- an increase in the vertical position of the maximum temperature from $y/D = 14$ to $y/D = 16.5$, and
- an increase in the spatial size of the plume.

The results of the temperature measurements in Fig. 5(b) show a similar trend with the flow measurements in Fig. 5(a). The temperature results observed here reflect previous work[27–29] that shows with the plume propagating downwind of the exhaust stack, a decrease in plume temperature and an increase in the height of the plume.

Downwind of the exhaust stack, the plume has a finite width in the span-wise direction, which was observed in the temperature measurements. Figure 6 shows the temperature contour plot along the X–Y plane at two different positions

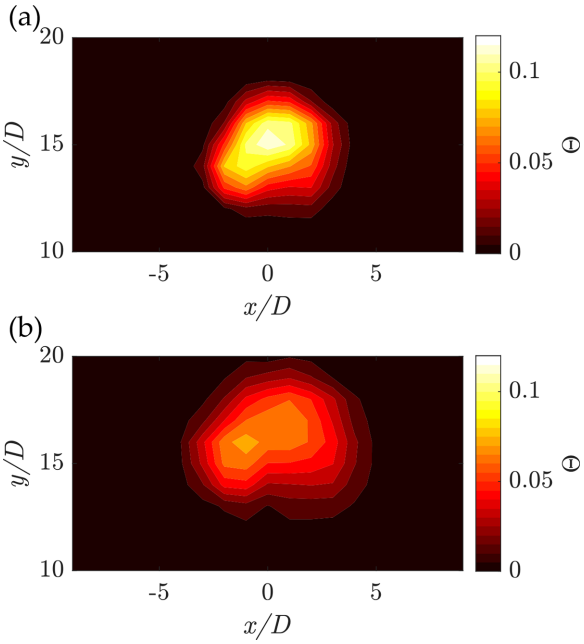

FIG. 6. (Color online) Experimental temperature contour plot from the non-isothermal JICF at various distance downwind from the exhaust stack (a) $z/D = 8$, and (b) $z/D = 16$, with $R = 5$, and $T_j = 500\,^{\circ}\mathrm{C}$.

https://doi.org/10.1121/10.0005489

downwind ($z/D = [8, 16]$). Figures 6(a) and 6(b) show similar features with the increase in distance from the exhaust stack downwind: a decrease in the maximum temperature of the plume, an increase in the height of the plume, and an increase in the spatial size of the plume. From measuring the temperature, the shape of the plume in Fig. 6 is similar to the counter-rotating vortex pairs observed in literature.[29] However, Fig. 6 shows that the maximum temperature was not in the middle of the plume, where the counter-rotating vortex is assumed to be, as observed in the literature.[29] There are a number of possible reasons for the unexpected position for the maximum temperature. One of the reasons could be simply experimental error in measuring the plume. Additionally, due to the discretised measurement, there could be a quantisation error in measuring the temperature at 1D intervals. Moreover, the duration for each temperature measurement (30 s) may be insufficient. Furthermore, the asymmetry bias in the plume could be related to asymmetry in the cross-flow or the jet. Without detailed flow measurements, it is not possible to definitively state that the temperature gradients observed are counter-rotating vortex pairs, but it is assumed based on the literature.[29]

In summary, the temperature measurements downwind of the exhaust stack exhibits the expected jet spreading and entrainment of the cooler cross-flow, and a reduction in the temperature gradients with distance. The results were only measured up to 16D due to the cost and availability of the wind tunnel. All the measurements show the presence of a thermal gradient, and if measurements were taken further downwind of the exhaust, the plume would dissipate further, where eventually the temperature downwind would be the same as the cross-flow free-stream temperature.

IV. ACOUSTIC RESULTS

The sound propagation through the exhaust is presented in this section for the following scenarios:

- sound propagation through an isothermal stagnant flow,
- sound propagation through a heated exhaust jet without cross-flow, and
- sound propagation through a heated elevated JICF.

Figure 7(a) shows the experimental results for the sound directivity at distances of 14D and 28D in the absence of the heated jet and cross-flow. As expected for the 4 kHz one-third octave band ($ka \approx 1.08$), the sound directivity is axisymmetric and elliptical, with a lobe forming along the centreline of the duct axis at 0°. The results in Fig. 7(a) show a very similar radiation pattern to published duct directivity in free-field environments.[31–33] This differs from the commonly used monopole assumption in ISO 9613-2:1996.[12] In Fig. 7(a), the elliptical lobe shows a reduction in sound levels of up to 4.5 dB at ±90° when compared to a monopole source with spherical spreading. Hence, for predictions of ground-level SPLs, the monopole assumption is likely to be conservative when designing noise control measures for neighbouring receivers.

Experiments were also conducted in an anechoic chamber for the previous scenario, to investigate the effects of testing in the wind tunnel, and the contribution from other reflective surfaces, such as the walls, ceiling, and the wind tunnel structure. The sound directivity results were almost identical to the results shown in Fig. 7(a). In addition, the authors also investigated the contributions from the reflections using temporal gating of the microphone signals. Temporal gating is a signal processing method in which sound that arrives within a specific time window is kept, and any signal arriving after that epoch is removed. When investigated, it was found that temporal gating made a negligible difference to the measurements and hence was not required for the final results.

Figure 7(b) shows the experimental results for the sound directivity at 28D with a heated jet of Mach number 0.1 and $T_j = 350\,°\text{C}$. The directivity plot shows that the sound is axisymmetric about the vertical axis, with a shadow zone or "cusp" forming along the centreline of the duct axis (0°). The acoustic cusp has a DI of approximately −12 dB. The acoustic energy that was originally on-axis has been refracted by the jet shear layer to form acoustic lobes off-axis at approximately symmetrical locations of ±50°. The SPL of the lobes off-axis has increased by approximately 3 dB, compared with Fig. 7(a). These results are qualitatively and quantitatively similar to work by others.[36–38,41] It should be noted that the experimental results in this study were measured at a lower jet temperature ($T_j = 350\,°\text{C}$) than commonly seen in OCGT exhaust stacks, and is a limitation of the experimental setup, where the air temperature at the 28D arc were not to exceed the 60 °C temperature rating of the microphones. While it was desirable to measure the directivity at 14D to observe the effects of distance on the sound propagation, in particular the refraction of sound as a result of the jet shear layer, unfortunately the microphone temperature limits were exceeded necessitating their removal during this test.

Figure 7(c) shows the experimental result for the sound directivity at 14D and 28D of a heated JICF with $M = 0.1$, $T_j = 500\,°\text{C}$, and R=5. Note that the cross-flow permitted higher stack exhaust temperatures than Fig. 7(b), while remaining under the 60 °C temperature limit at the microphone locations. By comparing Fig. 7(a) to 7(c), it can be observed that with the heated plume and cross-flow, the sound directivity is no longer elliptical or axisymmetric about 0°. The directivity of sound becomes biased towards the leeward side (or downstream) of the exhaust duct. The cross-wind shifts the peak observed in the downstream lobe from an angle from 65° to 90° for the 14D and 28D arrays, respectively. It can also be observed that as the sound propagates downstream, the width of the lobe decreases from 40° to 25° for the 14D and 28D arcs, respectively. Comparing the results from Figs. 7(a) and 7(c), as the downstream lobe bends over and becomes narrower, the energy becomes more concentrated, increasing in amplitude at the horizontal from –4.5 dB in Fig. 7(a) to 4.5 dB at 14D and 6.5 dB at 28D in Fig. 7(c). Hence, in Fig. 7(c), the plume has caused an

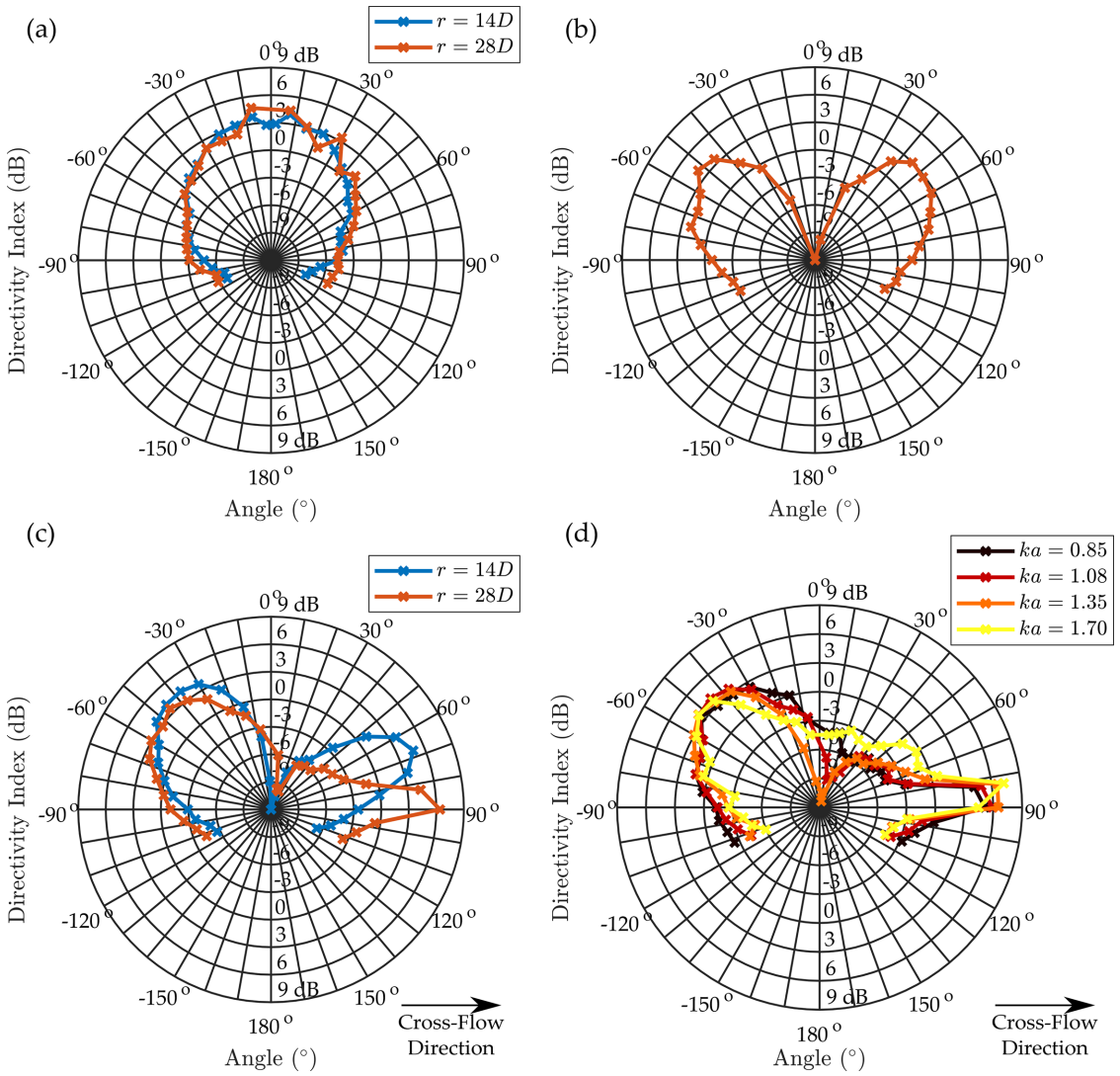

FIG. 7. (Color online) The DI for sound propagation in (a) an isothermal stagnant flow ($T_j = 27\,^{\circ}\mathrm{C}$), (b) a heated jet ($T_j = 350\,^{\circ}\mathrm{C}$) with no cross-flow, (c) a heated jet ($T_j = 500\,^{\circ}\mathrm{C}$) with cooler cross-flow at $ka = 0.85$, and (d) a heated jet ($T_j = 500\,^{\circ}\mathrm{C}$) with cooler cross-flow with $ka = [0.85, 1.08, 1.35, 1.70]$. The directivity results in (a), and (c) are for two different radii ($r = 14D$ and $28D$), where as the directivity results in (b) and (d) are for a single radius ($r = 28D$).

11 dB increase in the sound level parallel to the ground-plane when compared to the sound radiation in the absence of flow, as seen in Fig. 7(a). However, upstream of the exhaust duct, the sound directivity patterns remain similar for the $14D$ and $28D$ arcs. The position of the acoustic "cusp" or shadow zone shifted from 0° in Fig. 7(b) with no cross-flow to 10° at $14D$ and 20° at $28D$ with cross-flow present. It must be noted that the angular resolution of the directivity measurements is 7.5° increments and this may be insufficient in capturing fine detail in the directivity pattern. As sound propagates downstream, it can be observed that the plume continues to influence the propagation path and is strongly governed by the temperature gradients in the plume, which causes the sound to continually refract as it propagates downstream.

Figure 7(d) shows the directivity with varying band-averaged one-third octave bands ($f = [3.15, 4, 5, 6.3\,\mathrm{kHz}]$ or $ka = [0.85, 1.08, 1.35, 1.70]$) at radius of $28D$. All four curves show qualitative similarity in the acoustic results with: a cusp forming approximately at 10°, upwind of the exhaust stack a broad elliptical lobe resembling the off-axis lobe in Fig. 7(b) may be observed, and downwind a narrow acoustic lobe at approximately 90° forms. The key difference in directivity plots with the increase in acoustic frequency is the position of the acoustic lobe downwind, which shifts from 90° to approximately 80°. These results suggest that acoustic lobe downwind may not be fully resolved with the current angular spacing of the microphones. The results in Fig. 7(d) suggest that the directivity is dependant on the acoustic frequency. Jet temperature is an important parameter that governs the sound radiation downwind of the jet outlet and this parameter was also investigated. Figure 8(a) shows the directivity for the non-isothermal JICF, with $T_j = [27\,^{\circ}\mathrm{C}, 100\,^{\circ}\mathrm{C}, 300\,^{\circ}\mathrm{C}, 500\,^{\circ}\mathrm{C}]$. There are key features that remains the same in the directivity plots for all jet temperatures: a presence of a cusp on-axis (10°), a broad

https://doi.org/10.1121/10.0005489

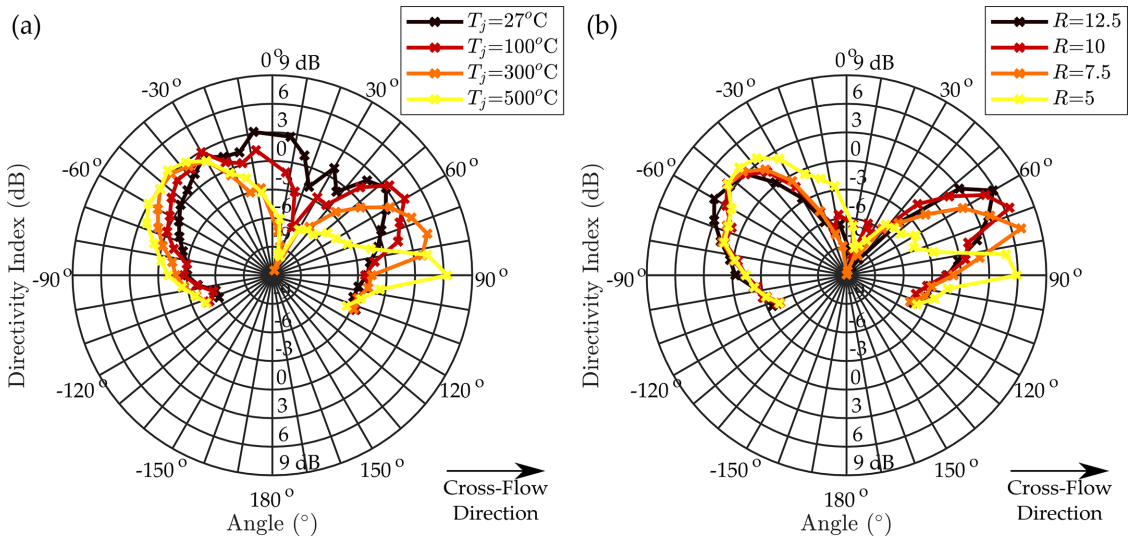

FIG. 8. (Color online) The DI along the *Y*–*Z* plane (of symmetry) for sound propagation through a non-isothermal JICF for band-averaged one-third octave bands for (a) varying jet temperature, T_j, for $R = 5$ and (b) varying cross-flow ratios, R, for $T_j = 500\,^{\circ}\mathrm{C}$. The following parameters were consistent and for all tests; centre frequency, $ka = 1.08$, and $r = 28D$. The cross-flow is going from left to right.

acoustic lobe upwind of the exhaust stack, and a concentration of sound downwind of the exhaust stack with narrow acoustic lobe. The increase in jet temperature shows unique temperature dependant features in the directivity plots, such as the following:

- the acoustic lobe position downwind of the exhaust stack shifts from approximately 50° to 90° with increasing temperature,
- the magnitude of the acoustic lobe downwind of the exhaust stack increases with temperature and can increase by up to approximately 4 dB from $T_j = 27\,^{\circ}\mathrm{C}$ to $500\,^{\circ}\mathrm{C}$,
- the depth of the cusp at approximately 7.5° to 22.5° increases with jet temperature, and
- upwind of the exhaust stack the magnitude of the lobe slightly increases with jet temperature.

Therefore, the jet temperature influences the directivity of sound, especially the refraction of sound downwind of the exhaust stack, with the hottest jet temperature ($T_j = 500\,^{\circ}\mathrm{C}$) showing the most significant increase in SPLs downwind by up to 9 dB.

Figure 8(b) shows the directivity for sound propagating through a non-isothermal jet in cross-flow with $R = [5, 7.5, 10, 12.5]$ and for a band-averaged one-third octave band ($f = 4$ kHz equivalent to $ka = 1.08$). The jet conditions remained fixed at $M = 0.1$ and $T_j = 500\,^{\circ}\mathrm{C}$, while the cross-flow free-stream velocity (u_{cf}) was varied to give the different values of R. The directivity plot shows that with a decrease in R from 12.5 to 5, the position of the acoustic lobe downwind shifts from 60° to 90°. While the increase in R towards 12.5 in Fig. 8(b) shows that the position of the acoustic lobe downwind becomes more axisymmetric with the upwind acoustic lobe about the jet centreline axis at 0°. The acoustic directivity for $R = 12.5$ almost resembles the sound directivity to Fig. 7(b), for $r = 28D$. The reason for similar directivity arcs is that with the reduction in cross-flow speed or increase in R, the plume downwind becomes more "jet dominant." In the relative near-field, the sound radiation at lower values of R or higher cross-flow free-stream velocities (u_{cf}) leads to the increase in SPL at ground-level ($28D$). In order to quantify the effects of the plume at these higher values of R, it is desirable to increase the spatial size of the experimental domain, but with the current facilities, this is not possible.

Figure 8(b) shows that the cross-flow momentum flux ratio, $R = 7.5$, produces the highest magnitude acoustic lobe downwind of the exhaust stack. However, given that the spatial resolution of the microphones was only 7.5°, the maximum detail of the acoustic lobe may not be resolved. Hence, the full SPL magnitude of the acoustic lobe, as well as other acoustic features may not have been captured with the current array configuration.

The geometry of the reduced scale mode exhaust stack is a simple straight duct section that protrudes $10D$ into the flow. In real OCGTs, the nearby plant equipment and buildings would affect the cross-flow and, consequently, the sound refraction. This simplification of the model is appropriate for scientific investigation, as it resembles elevated jets in cross-flow seen in literature and reduces the acoustic and fluid dynamic complexity in the model. The main purpose of this research was to investigate the sound interaction with the plume and observe non-axisymmetry of the acoustic directivity, as well as broadly quantify the increase in sound level downstream at the ground-level caused by refraction.

In the experimental work conducted here, measurements were taken with an anechoic ground to simulate an absorptive surface surrounding the stack. Reflective surfaces would change the sound directivity pattern, and hence the experimental setup used here may not be an accurate representation of real installations. Work completed by Leav *et al.*[43] suggests that a much more complex acoustic pattern

occurs when a reflective ground is included. As a result, Figs. 7 and 8 show "smooth" directivity patterns in the absence of diffraction and reflections from other surfaces. Additionally, the sound directivity results in this paper are presented over four different one-third octave band averages to reduce the complexity of the results. Further tests over additional one-third octave bands should be undertaken to examine the relationship of the plume and the downstream sound levels.

V. CONCLUSION

The experimental results presented in this paper have shown that under certain conditions, a heated jet in cooler cross-flow changes the propagation path of sound and can lead to increased sound levels observed downwind of the jet exhaust stack. The flow and temperature associated with the heated elevated JICF were measured and showed reproducible trends with the literature. Different operational conditions were investigated: the sound radiation through an isothermal stagnant flow, sound radiation in the presence of a heated jet without cross-flow, sound radiation in the presence of a heated JICF at $R = 5$, sound radiation with $T_j = [27\,^{\circ}\mathrm{C}, 100\,^{\circ}\mathrm{C}, 300\,^{\circ}\mathrm{C}, 500\,^{\circ}\mathrm{C}]$, and sound radiation cross-flow sensitivity study for a heated jet with cooler cross-flow, with $R = [5, 7.5, 10, 12.5]$. The key findings for the acoustic results are outlined below.

Downwind of the exhaust stack, the thermal and velocity gradients strongly refract the sound leading to the concentration of acoustic energy forming a narrow "lobe." The cusp previously seen on-axis for axisymmetric jets has rotated downwind by approximately 5°–10°. Downwind of the exhaust stack, the non-isothermal JICF can increase the observed DI by up to 11 dB when compared to the cases with the isothermal stagnant flow. The effects of the non-isothermal JICF are typically not considered for far-field sound level estimations with ISO 9613–1:1993[11] and ISO 9613–2:1996,[12] whereby the standards would underestimate the sound levels downwind of the exhaust stack.

The results presented in Fig. 8(a) highlights that the majority of the refraction arises from the temperature gradients, causing a change in the speed of sound $\left(\Delta c \propto \sqrt{\Delta T}\right)$, as opposed to the convective effects of the flow $(\Delta c = c + \Delta u_{\mathrm{flow}})$.[18] Therefore, the scenario with the hottest jet temperature $(T_j = 500\,^{\circ}\mathrm{C})$ shows the greatest asymmetry in the directivity plot. Downwind of the exhaust stack, the acoustic results show that an increase in T_j leads to an increase in the DI magnitude for the acoustic lobe downwind of the exhaust stack; downwind of the exhaust stack there is a shift in the position of the acoustic lobe towards the ground-plane; and upwind of the exhaust stack, the directivity lobe remains relatively unchanged with the change in jet temperature.

Work previously conducted by Leav *et al.*[43] showed that the counter rotating vortex pairs produce thermal and velocity gradients. In their numerical work, the refraction continued for the entire computational domain (40D downstream). Figure 7(c) shows the relationship with the plume development, and acoustic refraction is consistent with the experimental directivity measurements in this paper at 14D and 28D. Further experimental investigations will need to examine the directivity at distances greater than 28D to quantify the magnitude of the far-field directivity index. The flow and temperature fields associated with the experimental small-scale model will need to be measured to gain a better understanding of the fluid dynamics and temperature effects that govern the propagation path of sound.

The cross-flow sensitivity study provides insight into how the plume affects the sound. There are other factors that also change the position of the plume downwind, which include the terrain downstream and the turbulence intensity of the incoming flow. It was observed in previous research[27,28] for elevated jets in cross-flow that the incoming turbulence intensity influences the diffusion of the plume, as well as span-wise and vertical flapping motion of the plume in the incoming flow. Hence, a vertically flapping plume will cause the sound trajectory to change, and subsequently, the downwind lobe position will also vary. The work presented in this paper analysed the time-average response of the sound, temperature, and flow for an elevated jet in cross-flow. Hence, the transient effects of the sound interacting with the flapping plume were not quantified for this research.

The findings from this paper have highlighted the importance of accounting for the heated plume in cooler cross-flow when predicting the sound downwind of a hot exhaust stack.

ACKNOWLEDGMENTS

Leav was sponsored by an Australian Government Research Training Program Scholarship from 2015 to 2018.

[1]E. Björk, "Experimental study of measures to reduce noise radiated from power-station exhaust stacks," Noise Control Eng. J. **42**, 171–178 (1994).
[2]N. Broner, "A simple criterion for low frequency noise emission assessment," J. Low Freq. Noise Vib. Active Control **29**, 1–13 (2010).
[3]N. Broner, "A simple outdoor criterion for assessment of low frequency noise emission," Acoust. Austr. **39**, 7–14 (2011).
[4]N. Broner, "Power to the people," in *Proceedings of the 15th International Meeting on Low Frequency Noise and Vibration and Its Control*, Stratford upon Avon, United Kingdom (May 22–24, 2012), pp. 1–10.
[5]G. Hessler, Jr., "Proposed criteria in residential communities for low-frequency noise emissions from industrial sources," Noise Control Eng. J. **52**, 179–185 (2004).
[6]G. Hessler, Jr., "Proposed criteria for low frequency industrial noise in residential communities," Low Freq. Noise Vib. Active Control **24**, 97–106 (2005).
[7]R. Hetzel and R. Putnam, "Sources and rating criteria of low frequency gas turbine exhaust noise—Via case study," in *Proceedings of INTER-NOISE and NOISE-CON Congress and Conference Proceedings 2009*, Ottawa, Canada (August 23–26, 2009), pp. 1600–1607.
[8]G. Kudernatsch, "Combustion turbine exhaust systems-low frequency noise reduction," in *Proceedings of INTER-NOISE 2000, the 29th International Congress and Exhibition on Noise Control Engineering*, Nice, France (August 27–31, 2000), pp. 1–6.
[9]W. C. Lucas and G. F. Hessler, Jr., "The reduction of low frequency gas turbine exhaust noise: A case study," in *ASME 1996 International Gas*

Turbine and Aeroengine Congress and Exhibition, Turbo Expo: Power for Land, Sea, and Air, Birmingham, UK (June 10–13, 1996).
[10]J. R. Newman and K. I. McEwan, "Low frequency gas turbine noise," J. Eng. Power **102**, 476–481 (1980).
[11]ISO 9613-1:1993: *Acoustics—Attenuation of Sound During Propagation Outdoors – Part 1: Calculation of the Absorption by the Atmosphere* (ISO, Geneva, Switzerland, 1993).
[12]ISO 9613-2:1996: *Acoustics—Attenuation of Sound During Propagation Outdoors—Part 2: General Method of Calculation* (ISO, Geneva, Switzerland, 1996).
[13]ISO 10494:2018: *Gas Turbines and Turbine Sets—Measurement of Emitted Airborne Noise – Engineering/Survey Method* (ISO, Geneva, Switzerland, 2018).
[14]K. Attenborough, S. Taherzadeh, H. Bass, X. Di, R. Raspet, G. Becker, A. Güdesen, A. Chrestman, G. Daigle, and A. L'Espérance, "Benchmark cases for outdoor sound propagation models," J. Acoust. Soc. Am. **97**, 173–191 (1995).
[15]K. Attenborough, "Sound propagation close to the ground," Ann. Rev. Fluid Mech. **34**, 51–82 (2002).
[16]T. Embleton, "Tutorial on sound propagation outdoors," J. Acoust. Soc. Am. **100**, 31–48 (1996).
[17]U. Ingård, "A review of the influence of meteorological conditions on sound propagation," J. Acoust. Soc. Am. **25**, 405–411 (1953).
[18]V. Ostashev and D. Wilson, *Acoustics in Moving Inhomogeneous Media* (CRC Press, Boca Raton, FL, 2015).
[19]J. Piercy, T. Embleton, and L. Sutherland, "Review of noise propagation in the atmosphere," J. Acoust. Soc. Am. **61**, 1403–1418 (1977).
[20]M. Adaramola, D. Sumner, and D. Bergstrom, "Effect of velocity ratio on the streamwise vortex structures in the wake of a stack," J. Fluids Struct. **26**, 1–18 (2010).
[21]O. Eiff, J. Kawall, and J. Keffer, "Lock-in of vortices in the wake of an elevated round turbulent jet in a crossflow," Exp. Fluids **19**, 203–213 (1995).
[22]O. Eiff and J. Keffer, "On the structures in the near-wake region of an elevated turbulent jet in a crossflow," J. Fluid Mech. **333**, 161–195 (1997).
[23]O. Eiff and J. Keffer, "Parametric investigation of the wake-vortex lock-in for the turbulent jet discharging from a stack," Exp. Therm. Fluid Sci. **19**, 57– 66 (1999).
[24]R. Huang and R. Hsieh, "An experimental study of elevated round jets deflected in a crosswind," Exp. Therm. Fluid Sci. **27**, 77–86 (2002).
[25]R. F. Huang and R. H. Hsieh, "Sectional flow structures in near wake of elevated jets in a crossflow," Am. Inst. Aeronaut. Astronaut. J. **41**, 1490–1499 (2003).
[26]R. F. Huang and C. M. Hsu, "Turbulent flows of an acoustically excited elevated transverse jet," Am. Inst. Aeronaut. Astronaut. J. **50**, 1964–1978 (2012).
[27]J. Andreopoulos, "Wind tunnel experiments on cooling tower plumes: Part 1—In uniform crossflow," J. Heat Transfer **111**, 941–948 (1989).
[28]J. Andreopoulos, "Wind tunnel experiments on cooling tower plumes: Part 2—In a nonuniform crossflow of boundary layer type," J. Heat Transfer **111**, 949–955 (1989).
[29]B. E. Johnson, G. S. Elliott, and K. T. Christensen, "Structural characteristics of a heated jet in cross-flow emanating from a raised, circular stack," Exp. Fluids **54**, 1543 (2013).
[30]R. J. Wells and B. E. Crocker, "Sound radiation patterns of gas turbine exhaust stacks," J. Acoust. Soc. Am. **25**, 433–437 (1953).
[31]D. Bies, C. Hansen, and C. Howard, *Engineering Noise Control: Theory and Practice*, 5th ed. (CRC Press, Boca Raton, FL, 2017).
[32]A. Day and B. Bennett, "Directivity of sound from an open ended duct," in *Proceedings of AAS 2008*, Geelong, Victoria, Australia (November 24–26, 2008).
[33]A. Day, C. Hansen, and B. Bennett, "Duct directivity index applications," Acoust. Austr. **37**, 93–97 (2009).
[34]R. Amiet, "Refraction of sound by a shear layer," J. Sound Vib. **58**, 467–482 (1978).
[35]S. Candel, "Acoustic transmission and reflection by a shear discontinuity separating hot and cold regions," J. Sound Vib. **24**, 87–91 (1972).
[36]J. Atvars, L. Schubert, and H. Ribner, "Refraction of sound from a point source placed in an air jet," J. Acoust. Soc. Am. **37**, 168–170 (1965).
[37]J. Atvars, L. Schubert, E. Grande, and H. Ribner, *Refraction of Sound by Jet Flow or Jet Temperature* (Institute for Aerospace Studies, University of Toronto, Toronto, Canada, 1965).
[38]E. Grande, "Refraction of injected sound by a very cold nitrogen jet," J. Acoust. Soc. Am. **38**, 1063–1064 (1965).
[39]P. Mungur, H. Plumblee, and P. Doak, "Analysis of acoustic radiation in a jet flow enviroment," J. Sound Vib. **36**, 21–52 (1974).
[40]A. Cummings, "High temperature effects on the radiation impedance of an unflanged duct exit," J. Sound Vib. **52**, 299–304 (1977).
[41]R. J. Astley and W. Eversman, "Wave envelope elements for acoustical radiation in inhomogeneous media," Comput. Struct. **30**, 801–810 (1988).
[42]O. Leav, B. Cazzolato, and C. Howard, "Directivity analysis of sound in turbulent exhaust jets with laminar cross-flow: A numerical study," in *Proceedings of the Australian* Acoustics Society 2015, Hunter Valley, Australia (November 15–18, 2015), pp. 1–10.
[43]O. Leav, B. Cazzolato, and C. Howard, "A computational analysis of sound directivity from sound propagation through non-isothermal, turbulent exhaust jets in cross-flow," in *Proceedings of the 24th International Congress on Sound and Vibration*, London, UK (July 23–27, 2017), pp. 1–8.
[44]Siemens, "We power the world with innovative gas turbines—Siemens gas turbine portfolio," Data sheet (Siemens, Munich, Germany, 2019).
[45]J. Bendat and A. Piersol, *Engineering Applications of Correlation and Spectral Analysis*, 2nd ed. (John Wiley & Sons, New York, 1993).
[46]Y. Kamotani and I. Greber, "Experiments on a turbulent jet in a cross flow," Am. Inst. Aeronaut. Astronaut. J. **10**, 1425–1429 (1972).